Trends in the band structures of the group I and II oxides

Elisabeth A Mikajlo[a]
Department of Chemistry, Flinders University of South Australia, GPO Box 2100, Adelaide SA 5001, Australia

Helen E Dorsett
Defence Science and Technology Organisation, PO Box 44, Pyrmont, NSW 2009, Australia

Michael J Ford[b]
Institute for Nanoscale Technology, University of Technology, Sydney, PO Box 123, Broadway, NSW 2007, Australia

Abstract: Measured and calculated band structures for the six lightest Group I and II oxides are reported. Band structures have been measured using electron momentum spectroscopy, a technique that maps the ground state occupied orbitals resolved both in energy and momentum. Measurements are compared with first principles calculations carried out within the linear combination of atomic orbitals (LCAO) approximation using both Hartree-Fock (HF) and Density Functional methods (DFT). Three DFT functionals are used representative of the local density approximation (LDA), the generalised gradient approximation (GGA) and a hybrid method incorporating exact exchange. The calculated O 2p bandwidths and O 2p – 2s band gaps generally scale linearly with the inverse of the oxygen-oxygen separation squared, but consistently show an anomaly at Li_2O. These trends, including the anomaly, are also observed in the experimental data. HF calculations consistently overestimate the oxygen 2p - 2s band gap by almost a factor of 2. Measured band gaps lie within the range of the three DFT functionals employed, with evidence that the description of exchange becomes more important as the cation size increases. Both HF and DFT overestimate the oxygen

valence bandwidths, with DFT giving more accurate predictions. Both observed and calculated bandwidths converge as the cation size increases, indicating that exchange-correlation effects become less important as the metallic ion becomes larger.

[a] Present address: School of Chemistry, University of Nottingham, UK
[b] Corresponding author. Email address: mike.ford@uts.edu.au

I. INTRODUCTION

The Group I and II oxides are, in many respects, prototypical ionic solids. The lightest three from each group form a simple chemical series, all crystallising into the cubic *Fm3m* antifluorite or rocksalt structure, with the exception of BeO, which has a hexagonal structure. They all have a relatively small number of electrons in the unit cell, which makes them attractive for computational studies, since first principles calculations can be performed at a high level of theory with relatively modest resources. From an experimental point of view, a comprehensive data set across the two groups provides a standard for testing electronic structure methods applied to periodic systems with localised electrons. Despite this, there are virtually no measurements reported in the literature of the complete band structures, and indeed, very few measurements at all for the Group I oxides. Ultraviolet (UPS) and x-ray photoemission spectroscopy (XPS) have been used to probe oxidation of Li[1-3] , Na[4,5] or K[1,3,5,6] and the absorption of oxygen onto potassium covered surfaces of Pt, Fe and ZrC[7]. The core levels have been measured in electron emission by Barrie and Street[8] , and only recently densities of states in the valence and core regions of Li_2O have been reported by Tanaka *et al.*[9] and Liu *et al.*[10] using XPS and UPS. A number of optical[11], x-ray[12,13] and photoemission measurements[14,15] for the group II oxides have been available in the literature for some time, and provide data on only certain aspects of the electronic structure, such as special point energies. A notable exception is the more recent angle resolved photoemission measurement (ARPES) of MgO by Tjeng *et al.*[16]. Hence, calculations for ionic solids, unlike metallic or semiconducting solids, remain relatively untested.

The local density approximation[17] (LDA) of DFT continues to be the work horse of condensed matter calculations as there is no simple method available for including correlation into Hartree-Fock models for solids. However, one might expect the LDA to give a poor description of the strongly varying charge distribution found in ionic solids and that gradient

corrected[18] or hybrid functionals[19] are required. LDA predictions of optical band gaps and valence bandwidths are known to be problematic due to cancellation of self-energy terms in the Coulomb exchange potentials[20]. However, a general assessment of DFT and available functionals is not available for ionic systems. Previous theoretical studies, particularly for the group I oxides, have tended to focus on predicting lattice parameters[21,22] and optical band gaps[23], presumably because these quantities are readily available from previous experimental data and allow for some assessment of the success of the calculations. Nevertheless, the ability of a calculation to predict structural and elastic properties of solids reliably, as is the case for HF calculations of Group I oxides[21,22], does not necessarily mean it will provide an accurate description of their electronic structures.

It is clear from the cohesive energies that correlation effects are important and become more so as the size of the cation increases[21]. While these effects can, to some extent, be compensated in lattice parameter calculations (and other elastic properties) by using extended basis sets, it is unlikely that a Hamiltonian without correlation can provide reliable electronic structure predictions[24,25]. It is also clear that there is currently insufficient experimental evidence with which to test these aspects of any calculations.

In this work we present observed chemical trends in the oxygen valence band structures across the lightest Group I and Group II oxides. These are compared to calculations within the LCAO approximation to determine how accurately HF and DFT methods describe these trends in ionic solids. More crucially we can test whether the available exchange-correlation functionals of DFT are universal, and, if not, where they are best applied. We have published band structures for individual representatives of Group I [26] and Group II oxides[25], resolved both in energy and momentum using our technique of electron momentum spectroscopy, and accompanied with comparisons to theory. In this paper we present, for the first time, a complete and internally consistent set of experimental and calculated data and an analysis of

the trends in band structure observed for these six oxides. The calculations have been extended to provide a direct across-the-board comparison with measurement. From our analysis, we identify some of the strengths and shortfalls of current *ab initio* methods in predicting the electronic structure of these solids, and conclude that the EMS data set as a whole provides a benchmark for comparison with other theoretical calculations and measurements.

II. EXPERIMENTAL METHODS

In this section we discuss our spectroscopic technique, electron momentum spectroscopy (EMS), for measuring band structures and sample preparation. The aim is not to provide a detailed account of the methods, but rather highlight pertinent aspects of the experiment and make clear the information it provides and how this is analysed. Detailed accounts of the Flinders EMS apparatus[27,28] and the EMS technique[29] can be found elsewhere.

A. THE EMS TECHNIQUE

In its simplest conception, EMS is akin to playing "pool" or "billiards" with electrons. In billiards, an incident ball strikes a target and is scattered, with the two balls leaving the collision site at angles and energies uniquely defined by the energy loss of the incident ball and the momentum of the target ball before it was struck. Thus, if the target ball was moving before the collision, its momentum can be determined if the energy and momentum of the incident ball is known, and the energy and momentum of the two balls are measured after the collision. Although electron impact ionisation is inherently a quantum-mechanical phenomenon, this "classical" approach can be applied under the appropriate scattering kinematics, namely, a high incident energy and large momentum transfer.

This so-called (e,2e) reaction[29] is the essence of our experiment. A collimated 20.8 kV beam of electrons is aimed at the solid target to be investigated, and the ejected and scattered

electrons are detected within small energy windows centred nominally at 1.2 and 19.6 keV respectively and over a small range of azimuthal angles at fixed polar angles of 76° and 13.6° respectively relative to the path of the incident electrons. A coincidence pulse counting technique is used to determine pairs of electrons originating from a common collision event. The difference in arrival times at the electron detectors for correlated pairs will always be the same, whereas random pairs have random arrival times. Collecting data for a large number of collisions over a range of energy and momentum values directly maps the probability density of the target electrons in energy-momentum space.

A typical data set from the experiment is shown in the right panel of Fig 1. The greyscale map indicates how electrons within the target are distributed in energy and momentum, with darker colour representing a higher probability of finding an electron at that particular energy and momentum. The important point is that this is the direct output of the experiment. The energy scale is binding energy relative to the vacuum level of the spectrometer. Although absolute energies cannot reliably be determined without precise information about contact potentials and work functions (which vary with different targets), relative energies are readily derived from the spectra.

The momentum axis is the real momentum of the target electron. Fig. 1 bears a direct relationship to the more familiar band structure plots (or band dispersions) found in any undergraduate solid state text (see, for example Kittel p218[30]), but is slightly different. The latter show the distribution of electron orbitals in energy and momentum in the reduced zone scheme. Crystal momentum, rather than real momentum, is plotted and labelled in terms of the symmetry points of the reciprocal lattice. We plot the distribution of ground state occupied orbitals in the extended zone scheme.

EMS is a powerful technique because it can provide a direct measurement of the band dispersions and band occupation for crystalline or amorphous solids. Angle-resolved

photoemission can provide band dispersions, but intensities are difficult to extract from the measurement, and the technique is best applied to single crystalline solids. Other more conventional techniques, such as XPS, UPS, Compton profiles, integrate the band structure over one or more variables.

Due to our method of sample preparation (described in the next section) our samples are expected to be polycrystalline. Hence the energy-momentum map in Fig 1, and therefore the binding energy spectra in Fig 2, are a spherical average over all crystal directions. At zero momentum (the Γ-point) the bands are highly degenerate and spherical averaging will have little effect. Hence zero momentum band energies can be compared directly to other experiments and calculations. At all other momentum values, the dispersion relation is generally different along different directions, and band widths will be altered by spherical averaging, becoming narrower. We take account of this in our own calculations by a procedure described below.

In order to provide a quantitative comparison with calculation and other experimental results the data are analysed as follows. Vertical slices of a fixed momentum width (0.05 atomic units) are taken through the energy momentum maps of Fig. 1, yielding a series of binding energy spectra at different momentum values. The binding energy peaks in these spectra are then fitted to determine the peak positions. In the present paper we fit each peak with either one or two gaussians depending on the peak shape and fit quality, and fit the background with a fourth order polynomial. A linear least squares procedure is used, where the gaussian energy position and width and polynomial coefficients are the parameters determined by the fit. There is no *a priori* reason to choose these particular functions, beyond the fact that they give high quality fits where the error is dominated by the experimental resolution and not the fit itself. From this procedure we obtain numerical energy data that can be compared with theory and other experimental work. In particular we extract

intervalence band gaps and O 2p bandwidths. A typical binding energy spectrum is shown in Fig 2, together with the results of the least squares fit.

B. SAMPLE PREPARATION

The main limitation of our EMS technique is in the sample preparation. Because the spectrometer operates in transmission mode, targets must be no thicker than about 10 nm in order to achieve reasonable signal to background ratios. For thicker targets the signal is swamped by multiple scattering of the electrons. Although we have been able to produce 6 nm thick single-crystal free-standing targets of silicon[31], it is difficult to do the same for alkali oxide targets. Instead, we exploit the relative surface sensitivity of the spectrometer afforded by the low ejected electron energy, and prepare samples by evaporation onto a 3 nm thick amorphous carbon substrate. The result is a self-supporting target; The carbon substrate contributes only to the background, since the measured EMS signal originates entirely from the outermost 2 nm of the ultra-thin metal oxide film on the "electron-exiting" side of the target. Each of the oxides presented here, except BeO, are prepared by evaporation of the respective metal, through simple resistive heating, in an oxygen background of between 10^{-7} and 10^{-6} Torr. The typical background pressure in the vacuum chamber was 10^{-10} torr. It is necessary to prepare the BeO sample by repeated evaporation of the metal followed by heating in an oxygen background. Samples are prepared *in situ* and are transferred to the EMS measurement chamber entirely under UHV.

Sodium and potassium oxide are more difficult to prepare than Li_2O, or the Group II oxides since a number of oxide species are possible. During evaporation the flux of sodium or potassium and oxygen arriving at the surface is adjusted to give a metal rich deposition. Under these conditions one would expect formation of M_2O and perhaps some un-oxidised metal[3]. The Auger spectra taken after evaporation are consistent with a metal rich oxide.

There is no indication of un-oxidised metal in the EMS data, and the sodium oxide EMS spectra have a single, broad feature due to the O 2p states, indicating the presence of atomic, rather than molecular oxygen[1,3,5].

EMS measurements of these samples were conducted under UHV conditions with a typical pressure of 7 x 10^{-10} torr. The EMS experiment is not sensitive to surface contamination produced at this pressure. Measurements were typically conducted for three days in order to gain sufficient statistics, but due to sample degradation results presented are generally aggregates of identically prepared samples, with each sample run for approximately a day. Over this time scale no appreciable change in the EMS spectrum is observed. Although compared with conventional electron impact techniques this is an extremely long exposure time, the total electron dosage is small: incident beam currents in the EMS apparatus are typically less than 100 nA giving a total irradiation that is the same as a typical 10 min Auger measurement. No signs of sample charging, such as shifts or broadening of peaks, were observed during these measurements.

III. LCAO CALCULATIONS

The ground state electronic structures were calculated in CRYSTAL98[32] at both the HF and DFT levels. This is an *ab initio* LCAO calculation using gaussian type orbitals. Three DFT exchange-correlation functionals were used: the local density approximation (LDA) with Vosko-Wilk-Nusair exchange and correlation[17], the generalised gradient approximation with Perdew-Burke-Ernzerhof exchange and correlation (PBE)[33] and a hybrid method incorporating PBE exchange and correlation together with 25% exact HF exchange (PBE0)[34].

Calculations were performed with high quality all electron basis sets recommended by the authors of CRYSTAL98, and developed and optimised specifically for these oxides [21,35,36]. Dovesi *et al.*[21] have shown that these basis sets give reliable results for the group I oxides,

and that the addition of polarisation functions or a second valence shell has only minor effects on the elastic properties. We have also tested basis set effects on band energies and intensities: adding a *d* shell to either the anion or cation in lithium oxide (Li_2O) changes the band energies by <1%; and adding a second *sp* valence shell to the cation changes the energies by <2%. Band intensities essentially remain unchanged in all cases. Electronic structures were calculated using the characteristic crystal structure and experimental lattice parameters from Wyckoff[37]. Default tolerances for the CRYSTAL98 code were used throughout, with sufficient k-point sampling to ensure convergence of calculated properties.

As a preliminary test of the theoretical calculations, optimum lattice parameters for each of the oxides using the four different methods outlined above were calculated and compared with experimental values. The results are shown in Table I. The HF predictions fall within 10% of the experimental. This is not surprising given that the basis sets are optimised at the HF level. As expected LDA gives smaller lattice constants, gradient corrections expand the lattice and the hybrid method gives results that are similar to HF. For the band structure calculations we have used the experimental lattice constant from Wyckoff[37] rather than the optimised lattice constant in all cases. This makes negligible difference to the calculated electronic structures.

To compare our calculations directly with the EMS data, we must generate a spherically averaged energy-momentum map from the calculation. We achieve this by calculating along 25 evenly spaced crystal directions, which we find is sufficient to give a very good representation of the true spherical average over all crystal directions [24]. The calculated band dispersion relation and electron momentum density (EMD) for each of the 25 directions are combined to give the energy and momentum resolved probability density, and then summed to give the spherically averaged energy-momentum map. The results are then convoluted with gaussian functions of 1.0 eV and 0.1 a.u. FWHM, representing the experimental energy

and momentum resolutions respectively[27]. A typical result is shown in the left panel of Fig 1. The calculated, spherically averaged, energy-momentum map can now be analysed in exactly the same manner as the experimental data for a direct comparison.

IV. RESULTS AND DISCUSSION

A. GENERAL COMMENTS

Calculated and experimental energy-momentum maps for Li_2O shown in Fig. 1 are representative of the Group I and II oxides. Progressing down from low to high binding energies, the bands in Fig. 1 are derived predominantly from O 2p, O 2s and metal 1s atomic orbitals. Since they are highly ionic compounds (for example, the bond population in Li_2O is –0.01) there is little overlap between anion and cation orbitals, so the above assignments are close to the total orbital character of the bands.

The calculated spectrum (left panel) was produced by the hybrid DFT method, chosen for this example because it gives the closest match to experimental data for Li_2O (the other two DFT calculations give very similar results with only slight differences in the band energies). The theoretical results have been shifted in energy to match the observed electronic binding energy at the Γ-point of the O 2s band. With this normalisation, the hybrid DFT method reproduces the overall features of the O 2s and 2p valence bands, but is less accurate at predicting the observed energy gap between the O 2s and metal *s* bands.

Spectra for other oxides are qualitatively similar to Fig 1. For BeO and MgO, only the oxygen valence bands can be observed within a single energy window, the metallic core states being too low in energy. For CaO, Na_2O and K_2O, the metallic *p* and *s* bands are observed along with the oxygen valence bands.

A typical binding energy spectrum at an electron momentum of 0.4 a.u. is shown in Fig 2, with Li_2O again serving as the example. Spectra like this are derived from the energy-

momentum maps as discussed in Section II.A. Also shown are the results of fitting (and subsequently subtracting) the background in the spectrum using a fourth order polynomial. The background arises from random events and from multiple scattering of the incident and outgoing electrons due to plasmon excitation, valence electron excitation, or small-angle inelastic scattering. Studies using Monte Carlo simulations to generate a multiple scattering background for calculated spectra[24] indicate that multiple scattering has only a small effect on band energies derived from EMS data. The least squares fit to the background subtracted data is also shown. Finally, overlaid on the raw and background-subtracted experimental data of Fig. 2 is the spherically-averaged theoretical binding energy spectrum calculated from the hybrid DFT method, and normalised to the observed O 2s Γ-point. As in Fig. 1, the difference between predicted and observed O 2s - metal 1s band gaps is clearly evident, as are discrepancies between predicted and observed intensities, particularly for the O 2p and metal *s* bands.

Peaks in the binding energy spectrum are fitted to gaussian functions to extract the band dispersion (*i.e*., the electron binding energy as a function of momentum), and, consequently, the electronic band gaps and bandwidths. Band gaps at the Γ-point (zero momentum) are listed in Table II. Both the experimental and theoretical results are derived from spherically averaged data, however due to the degeneracy of bands at the Γ-point, the effect of the spherical averaging is minimal. At the Γ-point, we find that band gaps calculated from spherically-averaged results and those calculated from dispersion curves generated along particular crystalline directions differ by less than 1%, which in most cases is less than our quoted experimental error of ± 0.2 eV. Only calculated band gaps are given for K_2O because the exact position of the O 2s band is obscured by overlapping K *p* bands.

For the Group II oxides, there are a limited number of published values for the oxygen intervalence band gap based upon x-ray and photoemission measurements[12,14,15], studies have

generally concentrated on the valence-conduction band gap. The results in Table II are consistent with these reported values (see Sashin *et al.* for a detailed account[25]). For Group I oxides, the authors know of no previous experimental work with which to compare. A limited number of measurements exist, but these have reported only the O 2p band or cation core states. Where available, previous experimental measurements of core level energies[4,8,15] agree with our results. The calculated band gaps in Table II are consistent with results published by other groups.

Oxygen 2p bandwidths for Group I and II oxides are presented in Table III. Theoretical bandwidths derived both from spherically averaged calculations and from band extrema along a single crystalline direction where the band dispersion is greatest are given. Spherically averaged bandwidths are always narrower. The O 2s bandwidths have not been included since these are in most cases too narrow to be of use in assessing chemical trends among the six oxides. The cation core levels are also narrow as there is little overlap of these atomic-like core orbitals between neighbouring atoms. The experimental error of ± 0.2 eV quoted in Table III is based upon the resolution of the EMS spectrometer and the reliability of the peak fitting procedure for the binding energy spectra.

B. TRENDS IN THE OXIDE VALENCE BAND STRUCTURE

In a simple tight-binding model of metal oxides, the structure of the valence bands is determined by the difference in energy between the *s* and *p* orbitals on a single oxygen ion, and the inter-atomic matrix elements. These are very ionic compounds, so to a good approximation the metal-ion *s* band is unoccupied and pushed up into the conduction region. Therefore, the intervalence band gap depends upon overlap between adjacent oxygen ions and not nearest neighbour interactions with the metal cations. If the interatomic interactions

scale linearly with the reciprocal of this oxygen-oxygen distance squared[38] then the band gap should show a linear dependence on this quantity.

To test this assumption, measured and calculated O 2s – O 2p spherically-averaged band gaps (at the Γ-point) were plotted as a function of inverse-square oxygen distance (Fig. 3). Although the solids have differing structures, they can all be considered close-packed oxygen ion lattices with metal cations filling either the octahedral or tetrahedral holes depending upon their valency and ionic radius. Hence, simplistically, it is reasonable to expect a single linear trend across all six oxides rather than, say, independent trends for the anti-fluorite, rocksalt, and wurtzite structures.

There is a strong linear dependence in the data presented in Fig 3, with the notable exception of lithium oxide. This anomaly is present in both the experimental data and all of the calculations. The anomaly does not occur because there are two independent overlapping series - a straight line fit to the five calculated data points (Li_2O excluded) is considerably better than independent fits of the Group I and Group II oxides - but rather, from the physical properties of the oxides. The ionic radius of the lithium ion is smaller than the calcium ion, but its single valency necessitates occupancy of tetrahedral sites in the oxygen sub-lattice, thus forcing near-neighbour oxygens further apart. This anomaly in Li_2O is also apparent in other properties across the Group I and II oxides, such as Pauling electronegativities. Similar trends are observed in the spherically-averaged O 2p bandwidths (Fig. 4), which like the band gap, will depend upon near-neighbour oxygen atom interactions. The anomaly is more apparent in the maximal bandwidths derived from non-spherically-averaged calculations and plotted in Fig. 5. The calculated data shown here again fall on a reasonable straight line except for Li_2O. The K_2O point is raised slightly because the band structure has a different shape for this oxide due to the large size of the cation. Unlike the other five oxides considered, the oxygen 2p band in K_2O does not have its band edge at the

Γ-point. Spherical averaging of the bandwidth data as presented in Fig 4 tends to 'smear out' the effect.

C. RELATIVE PERFORMANC OF *AB INITIO* METHOD

Of the methods used in this study, HF calculations give the poorest predictions for O 2s – O 2p valence band gaps and O2p bandwidths of the Group I and II oxides. With the appropriate basis sets, the HF method is extremely good at predicting structural parameters for these ionic compounds, however, it consistently overestimates the oxygen band gap by approximately 30%. Correlation effects, particularly intra-ionic correlations[39], are important in these compounds, and DFT gives far better agreement with EMS measurements.

The observed oxygen band gaps fall within the predictions of the various DFT methods used in this study. For the smaller metallic ions (BeO, MgO), LDA and GGA functionals yield better agreement with experiment, whereas for CaO and Na_2O, better agreement is obtained with inclusion of exact exchange. The predicted O 2s – O 2p band gap for Li_2O is also marginally better with the hybrid functional. Thus the trend is that the description of exchange becomes relatively more important as oxygen-oxygen distance (or cation size) increases. This trend may be a manifestation of incomplete cancellation of the coulomb and exchange self-energy terms – a well-known problem in LDA calculations.

Returning to the band gap data of Table II, the experimental cation *s-p* band gap in Na_2O and CaO is again overestimated by HF and lies closer to the DFT calculations. The hybrid method gives the best prediction for Na_2O while the GGA performs marginally better for CaO. For the cation *p* to anion *s* band gap in Li_2O and Na_2O, all the calculations underestimate the experimental value, with HF giving the closest agreement. This band gap is also underestimated by all the calculations for CaO, but in this case, the HF value is smaller than all three DFT values, with GGA and LDA giving the closest predictions. As

discussed in Section IV.A experimental band gaps for K_2O are not given because of overlap of the O 2s and K 3p bands. HF predicts a clear separation between these bands whereas at the DFT level they overlap[26].

Unlike the band gaps plotted in Fig 3, experimental O 2p bandwidth data lie below all of the theoretical results, even after spherical averaging of the calculations that reduces the predicted bandwidths. This is rather unexpected, and our experimental values also fall below previous measurements. However, previous data are generally derived from the width of the DOS measured by photoemission[10,14,15], and there is no generally accepted rule for determining the bandwidth by this method. As Erwin and Lin[40] point out, care must be exercised in comparing such bandwidths with other data because they may overestimate the true width.

As with the band gaps, HF bandwidths are the least accurate, being consistently larger than bandwidths predicted by the three DFT methods. However, it is interesting to note that all bandwidth calculations converge to about the same value at K_2O. This might be interpreted as the decreasing importance of correlation with increasing cation size, resulting in less orbital overlap between neighbouring oxygen ions. By contrast, the calculated band gaps maintain almost constant spacing across the entire series of oxides, indicating a stronger dependence upon the 2s – 2p splitting on the oxygen ion rather than on interatomic overlap. Presumably, the band gaps are converging to the 2s – 2p splitting of an isolated oxygen ion.

V. CONCLUSIONS

Following on from a previous report on EMS of Group II oxides[25], we have combined our measurements for Group I and Group II oxides to study trends in their valence band structures. The results of this paper are derived from a complete analysis of the six oxides that allows direct comparison between current theory and experiment, and is applied

consistently across the whole data set. The strength of the EMS technique is its ability to probe the bandstructures of these highly insulating compounds without being limited to measurements of "special points" (as with optical and photoemission techniques), or the use of single-crystal samples. With the relatively minor additional step of spherically averaging calculations over several crystalline directions, state-of-the-art *ab initio* methods can be compared directly to experimental results.

Obvious criticisms of the EMS technique focus upon its unusual method of sample preparation (*i.e.*, can the electronic structures of ultrathin films be representative of the "true" solid?) and the possible influence of surface contamination (or the carbon substrate) upon the resulting measurements. However, we conclude that these effects are minimal, based upon similarities between the expected and observed chemical trends for EMS measurements. Plotted as a function of inverse-squared oxygen-oxygen distance, we find that EMS band gaps reproduce the gross trends of Group I and II oxide valence bands, including an expected anomalous "dip" in energy at Li_2O. Similar agreement is observed for EMS bandwidths: the bandwidths increase monotonically with decreasing oxygen distance due to increasing orbital overlap between near-neighbours.

Furthermore, we find that the resolution of the EMS technique is good enough for critical comparison with *ab initio* calculations. For instance, all but two predicted band gaps (PBE0/Na_2O(O 2s – O 2p) and GGA/CaO(Ca 3p – Ca 3s)) fall outside experimental error, and no single method consistently reproduces the observed trend of O 2s – O 2p band gaps versus inverse-squared oxygen distance. For smaller oxygen distances, (MgO and BeO) the GGA approximation gives the best agreement with experiment, while at larger distances the hybrid functional is more accurate. The observed trend highlights known deficiencies with density-functional methods, and could be used to improve existing theory.

Finally, we note that none of the *ab initio* techniques used in this paper reproduce the O 2p valence bandwidth, even when spherically averaged, although the GGA DFT approximation yields the best agreement for all oxides. Differences are most pronounced for the "intermediate" oxides, CaO and Li_2O, which fall between limits of low and high degrees of orbital overlap between neighbouring oxygens. Given the limited success with which the chosen *ab initio* methods were able to model the O 2s – O 2p band gaps, we assert that EMS measurements of ultrathin oxide films are a close representation of the band structure of the bulk solids, and that better agreement between calculations and experiment can be achieved with improvements to *ab initio* theory.

ACKNOWLEDGEMENTS

This work was supported by the University of Technology Sydney, the Flinders University of South Australia, and by the ARC. EAM was supported by a SENRAC scholarship. This work would not have been possible without the support of the workshop staff at Flinders University. Calculations were performed on the Chemistry Computing Cluster at Adelaide University and the ac3 facility in NSW. The authors acknowledge computing support from Jeff Borkent, Mark Buntine and Richard Leow.

REFERENCES

[1] S. L. Qiu, C. L. Lin, J. Chen, and M. Strongin, Phys. Rev. B **41** (11), 7467 (1990).

[2] S. L. Qiu, C. L. Lin, J. Chen, and M. Strongin, Phys. Rev. B **39** (9), 6194 (1989).

[3] J. Jupille, P. Dolle, and M. Besancon, Surf. Sci. **260**, 271 (1992).

[4] M. L. Shek, Hrbek, J., Sham, T. K. and Xu, G.-Q., J. Vac. Sci. Technol., A **9** (3), 1640 (1991).

[5] E. Bertel, F. P. Netzer, G. Rosina, and H. Saalfeld, Phys. Rev. B **39** (9), 6082 (1989).

[6] L.-G. Petersson and S.-E. Karlsson, Phys. Scr. **16**, 425 (1977); A. P. Baddorf and B. S. Itchkawitz, Surf. Sci. **264**, 73 (1992); B. Lamontagne, F. Semond, and D. Roy, Surf. Sci. **327**, 371 (1995).

[7] G. Broden, G. Pirug, and H. P. Bonzel, Chem. Phys. Lett. **73** (3), 506 (1980); M. Ayyoob and M. S. Hegde, Surf. Sci. **133**, 516 (1983); K. Ozawa, T. Noda, T. Nakane, K. Edamoto, and S. Tanaka, Surf. Sci. **438**, 223 (1999).

[8] A. Barrie and F. J. Street, J. Electron Spectrosc. Relat. Phenom. **7**, 1 (1975).

[9] S. Tanaka, M. Taniguchi, and H. Tanigawa, J. Nucl. Mater., 1405 (2000).

[10] L. Liu, V. E. Henrich, W. P. Ellis, and I. Shindo, Phys. Rev. B **54**, 2236 (1996).

[11] D. M. Roessler and W. C. Walker, Phys. Rev. **159** (3), 733 (1967); M. L. Cohen, P. J. Lin, D. M. Roessler, and W. C. Walker, Phys. Rev. **155** (3), 992 (1967); D. M. Roessler and W. C. Walker, Phys. Rev. Lett. **17** (6), 319 (1966); R. O. Whited and W. C. Walker, Phys. Rev. **188** (3), 1380 (1969); R. C. Whited, C. J. Flaten, and W. C. Walker, Solid State Commun. **13**, 1903 (1973); D. M. Roessler, W. C. Walker, and E. Loh, J. Phys. Chem. Solids **30**, 157 (1969); M. L. Bortz, R. H. French, D. J. Jones, R. V. Kasowski, and F. S. Ohuchi, Phys. Scr. **41**, 537 (1990).

[12] V. A. Fomichev, Sov. Phys. - Sol. Stat. **13** (3), 754 (1971); A. P. Lukirskii and I. A. Brytov, Sov. Phys. - Sol. Stat. **6** (1), 33 (1964).

[13] V. A. Fomichev, T. M. Zimkina, and I. I. Zhukova, Sov. Phys. - Sol. Stat. **10** (10), 2421 (1969).

[14] L. Fiermans, R. Hoogewijs, G. d. Meyer, and J. Vennik, Phys. Status Solidi B **A59**, 569 (1980).

[15] H. Van Doveren and J. A. Verhoeven, J. Electron Spectrosc. Relat. Phenom. **21**, 265 (1980).

[16] L. H. Tjeng, A. R. Vos, and G. A. Sawatzky, Surf. Sci. **235**, 269 (1990).

[17] S. H. Vosko, L. Wilk, and M. Nusair, Can. J. Phys. **58**, 1200 (1980).

[18] J. P. Perdew, in *Electronic Structure of Solids '91*, edited by P. Ziesche and H. Eschrig (Akademie Verlag, Berlin, 1991).

[19] D. C. Langreth and M. J. Mehl, Phys. Rev. B **28** (4), 1809 (1983); V. Sahni, J. Gruenebaum, and J. Perdew, Phys. Rev. B **26** (8), 4371 (1982); H. Ou-Yang and M. Levy, Phys. Rev. Lett. **65** (8), 1036 (1990).

[20] F. Aryasetiawan and O. Gunnarsson, Rep. Prog. Phys. **61**, 237 (1998).

[21] R. Dovesi, C. Roetti, C. Freyria-Fava, and M. Prencipe, Chem. Phys. **156**, 11 (1991).

[22] R. Dovesi, Solid State Commun. **54** (2), 183 (1985).

[23] Y. N. Zhuravlev, Y. M. Basalaev, and A. S. Poplavnoi, Russian Physics Journal **44** (4), 398 (2001).

[24] B. Soule de Bas, H. E. Dorsett, and M. J. Ford, J. Phys. Chem. Solids **64**, 495 (2003).

[25] V. A. Sashin, H. E. Dorsett, M. Bolorizadeh, and M. J. Ford, J. Chem. Phys. **113**, 8175 (2000).

[26] E. A. Mikajlo and M. J. Ford, J. Phys.: Condens. Matter **15**, 6955 (2003); E. A. Mikajlo, K. L. Nixon, V. A. Coleman, and M. J. Ford, J. Phys.: Condens. Matter **14**, 3587 (2002); E. A. Mikajlo, K. L. Nixon, and M. J. Ford, J. Phys.: Condens. Matter **15**, 2155 (2003).

[27] S. A. Canney, M. J. Brunger, I. E. McCarthy, P. Storer, S. Utteridge, M. Vos, and E. Weigold, J. Electron Spectrosc. Relat. Phenom. **83**, 65 (1997).

[28] P. Storer, R. S. Caprari, S. A. Clark, M. Vos, and E. Weigold, Rev. Sci. Instrum. **65** (7), 2214 (1994).

[29] M. A. Coplan, Moore, J. H., and Doering, J. P., Reviews of Modern Physics **66** (3), 985 (1994); J. R. Dennison and A. L. Ritter, J. Electron Spectrosc. Relat. Phenom. **77**, 99 (1996); I. E. McCarthy and E. Weigold, Rep. Prog. Phys. **54** (6), 789 (1991).

[30] C. Kittel, *Introduction to solid state physics*. (Wiley, New York, 1996).

[31] S. J. Utteridge, V. A. Sashin, S. A. Canney, M. J. Ford, Z. Fang, D. R. Oliver, M. Vos, and E. Weigold, App. Surf. Sci. **162-163**, 357 (2000).

[32] V. R. Saunders, R. Dovesi, C. Roetti, M. Causà, N. M. Harrison, R. Orlando, and C. M. Zicovich-Wilson, *CRYSTAL98 User's Manual*. (University of Torino, Torino, 1998).

[33] J. P. Perdew, K. Burke, and M. Ernzerhof, Phys. Rev. Lett. **77** (18), 3865 (1996).

[34] M. Ernzerhof and G. E. Scuseria, J. Chem. Phys. **110** (11), 5029 (1999).

[35] A. Lichanot, M. Chaillet, C. Larrieu, R. Dovesi, and C. Pisani, Chem. Phys. **164**, 383 (1992).

[36] M.-P. Habas, R. Dovesi, and A. Lichanot, J. Phys.: Condens. Matter **10**, 6897 (1998).

[37] R. Wyckoff, *Crystal Structures*. (Interscience, New York, 1963).

[38] W. A. Harrison, *Electronic structure and the properties of solids*. (Dover, New york, 1989).

[39] K. Doll, M. Dolg, P. Fulde, and H. Stoll, Phys. Rev. B **52** (7), 4842 (1995); K. Doll, M. Dolg, and H. Stoll, Phys. Rev. B **54**, 13529 (1996).

[40] S. C. Erwin and C. C. Lin, J. Phys. C: Sol. Stat. Phys. **21**, 4285 (1988).

[41] S. Hull, T. W. D. Farley, W. Hayes, and M. T. Hutchings, J. Nucl. Mater. **160**, 125 (1988).

Table I. Calculated and experimental lattice parameters (Å). Values in parenthesis are experimental values extrapolated to the athermal limit.

	HF	LDA	GGA	HYBRID	EXP	
Li_2O	4.580	4.519	4.638	4.584	4.619[a]	(4.573)[b]
Na_2O	5.497	5.393	5.559	5.498	5.55[a]	(5.49)[c]
K_2O	6.466	6.168	6.414	6.360	6.436[a]	(6.38)[c]
BeO	2.685	2.661	2.705	2.683	2.698[a]	(2.675)[d]
	4.338	4.302	4.365	4.331	4.38[a]	(4.344)[d]
MgO	4.190	4.162	4.245	4.199	4.211[a]	-
CaO	4.847	4.699	4.811	4.783	4.81[a]	-

[a]Reference[37]

[b]Reference[41]

[c]Reference[21]

[d]Reference[35]

Table II. Γ-point band gaps (eV) derived from EMS and spherically averaged calculations. Error in the experimental values is ± 0.2 eV.

		HF	LDA	GGA	Hybrid	Exp
Li_2O	O 2p - O 2s	21.10	15.07	15.21	16.72	16.1
	O 2s – Li 1s	32.40	27.00	27.80	28.80	34.3
Na_2O	O 2p - O 2s	20.18	14.19	14.59	15.98	15.9
	O 2s – Na 2p	9.40	7.60	7.40	8.00	11.7
	Na 2p – Na 2s	34.80	24.40	28.00	29.60	31.5
K_2O	O 2p - O 2s	19.21	13.40	13.80	15.30	-
	O 2s – K 3p	2.47	0.6	0.6	2.02	-
	K 3p – K 3s	22.07	15.80	16.00	18.20	-
BeO	O 2p – O 2s	24.93	18.29	18.50	20.22	19.0
MgO	O 2p – O 2s	23.08	16.97	17.05	18.67	17.6
CaO	O 2p – O 2s	21.19	15.07	15.29	16.84	16.5
	O 2s – Ca 3p	1.12	3.24	3.24	2.9	3.8
	Ca 3p – Ca 3s	24.49	18.59	18.76	20.30	18.9

Table III. O 2p valence band widths (eV). Values in parenthesis are derived from the non-spherically averaged data. Error in the experimental values is ± 0.2 eV.

	HF	**LDA**	**GGA**	**HYBRID**	**EXP**
Li_2O	2.69 (3.50)	2.12 (2.82)	2.04 (2.76)	2.27 (3.03)	1.3
Na_2O	1.25 (1.72)	1.01 (1.47)	1.02 (1.42)	1.10 (1.55)	0.6
K_2O	0.38 (0.83)	0.37 (0.79)	0.30 (0.75)	0.39 (0.79)	0.3
BeO	6.77 (8.05)	5.39 (6.43)	5.30 (6.36)	5.75 (6.88)	4.7
MgO	4.54 (5.83)	3.61 (4.70)	3.64 (4.61)	3.89 (5.00)	3.3
CaO	2.33 (3.34)	1.80(2.71)	1.74 (2.61)	2.04 (2.89)	0.9

FIGURE CAPTIONS

FIG. 1. Experimental (right panel) and calculated (left panel) energy-momentum resolved band maps for Li_2O. Experimental binding energies are relative to the vacuum level of the spectrometer and for ease of comparison the calculated energies have been normalised to the experiment at the Γ-point of the O 2s band. Momenta are given in atomic units (a.u.).

FIG. 2. Experimental and calculated binding energy profiles for Li_2O at a momentum of 0.4 atomic units (a.u.). Binding energies are relative to the vacuum level of the spectrometer. Calculated binding energies and intensities have been normalised to the experiment at the O 2s peak at zero momentum

FIG. 3. Measured and calculated (spherically averaged) oxygen 2s – 2p band gaps. *d* is the nearest neighbour oxygen distance.

FIG. 4. Measured and calculated (spherically averaged) oxygen 2p bandwidths. *d* is the nearest neighbour oxygen distance.

FIG. 5. Calculated (non-spherically averaged) oxygen 2p bandwidth. *d* is the nearest neighbour oxygen distance.

FIG 1 E A Mikajlo et. al.
Journal of Chemical Physics

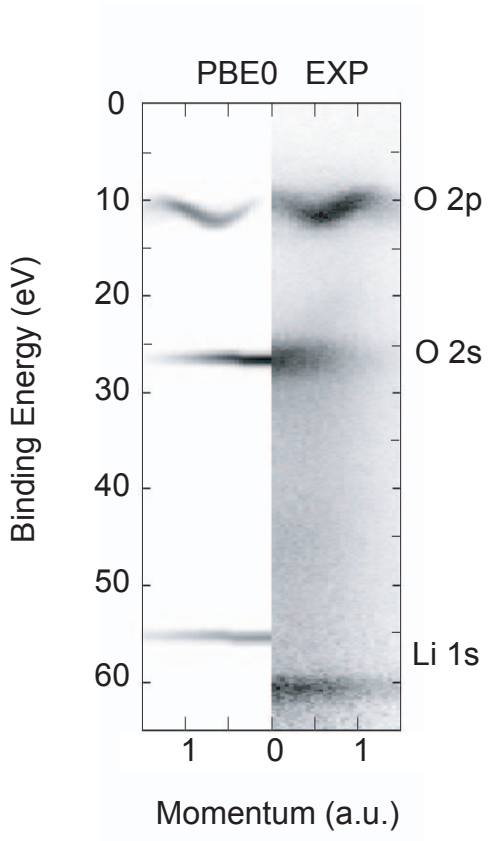

FIG 2 E A Mikajlo et. al.
Journal of Chemical Physics

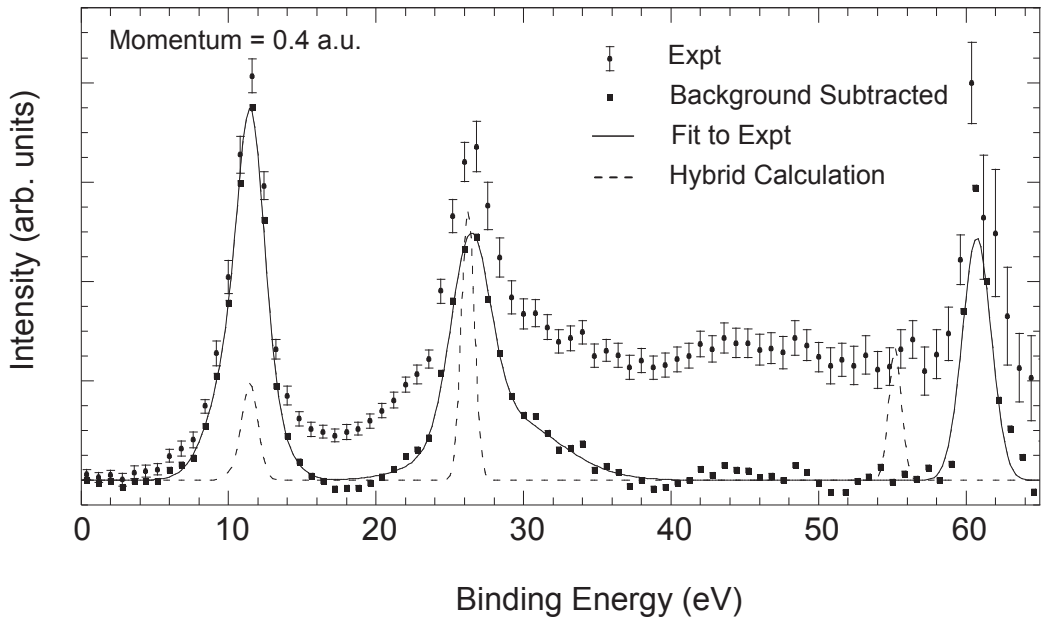

FIG 3 E A Mikajlo et. al.
Journal of Chemical Physics

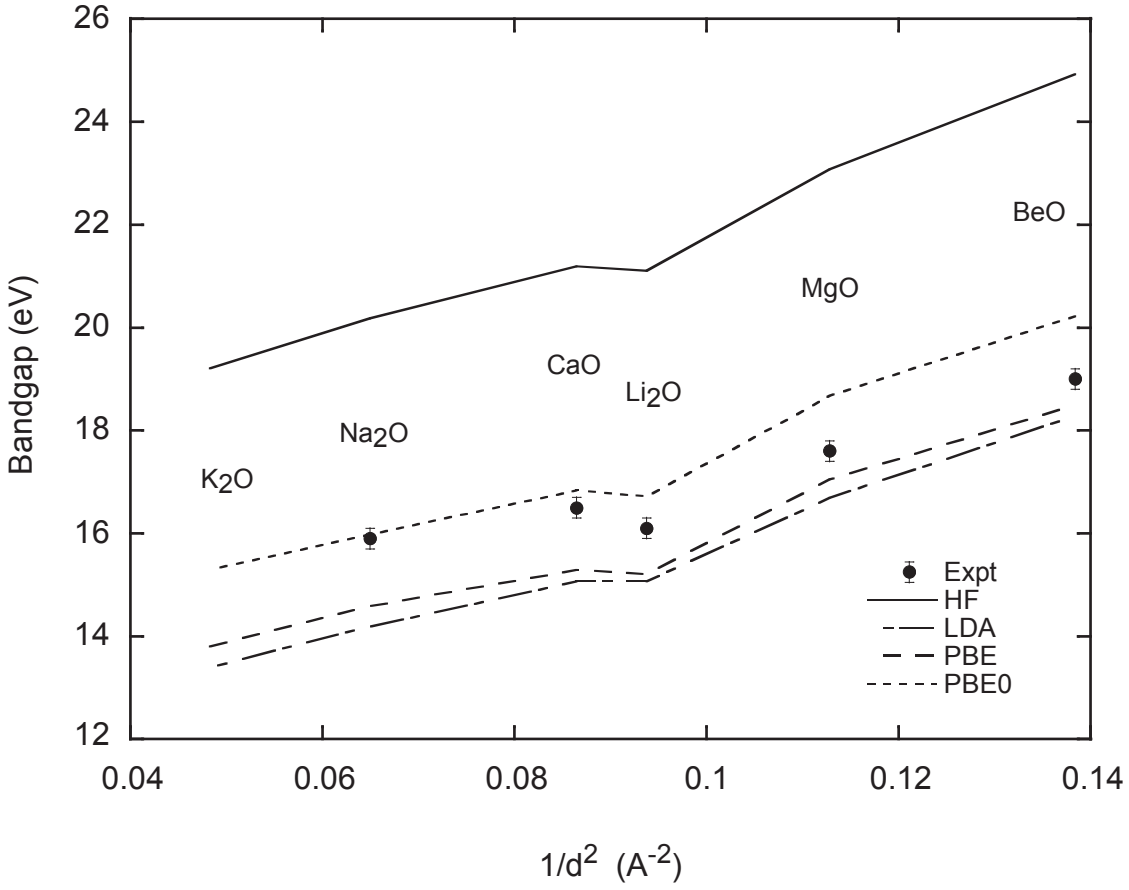

FIG 4 E A Mikajlo et. al.
Journal of Chemical Physics

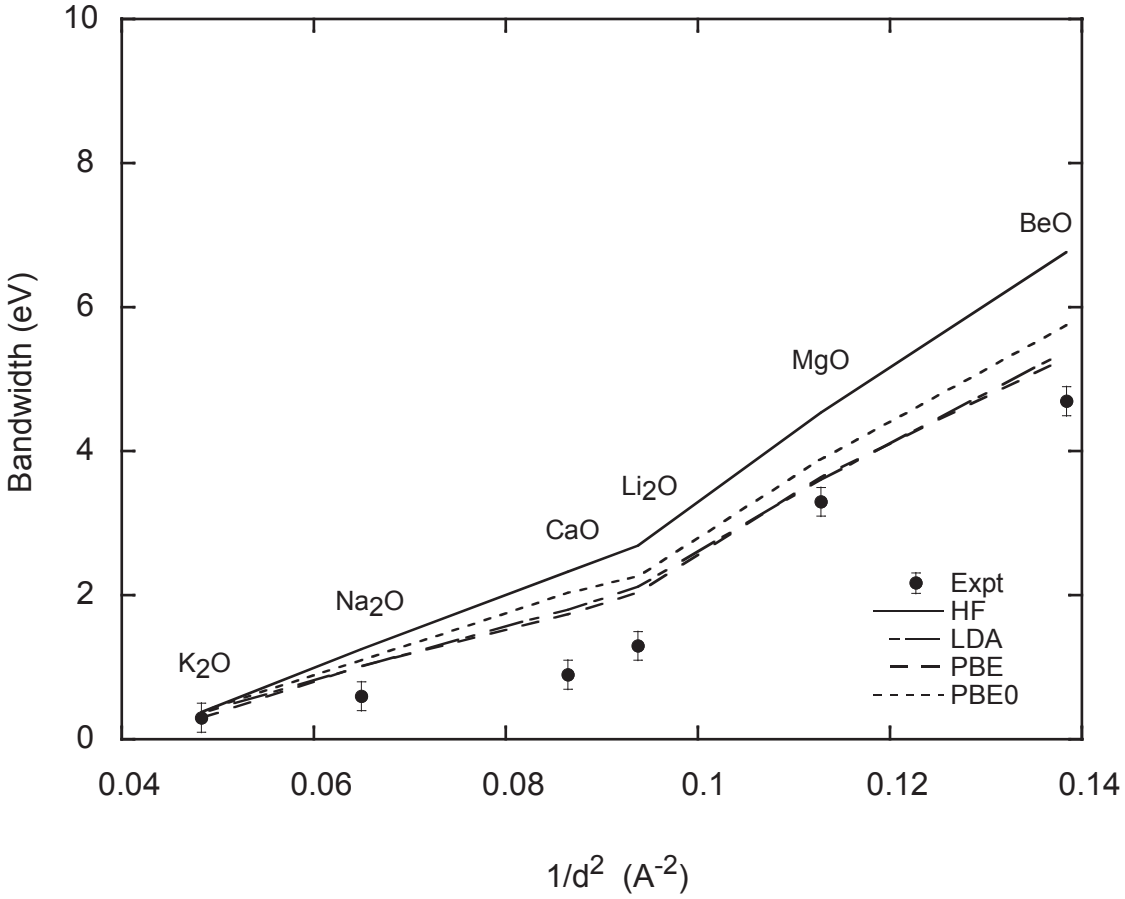

FIG 5 E A Mikajlo et. al.
Journal of Chemical Physics